

The importance of travelling wave components in standing surface acoustic wave (SSAW) systems[†]

CITSABEHSAN DEVENDRAN^a

LMS, Monash University

THOMAS ALBRECHT^b

Monash University

JASON BRENNER^a

LMS, Monash University

TUNCAY ALAN^a

LMS, Monash University

ADRIAN NEILD^{a*}

LMS, Monash University

I. SUPPLEMENTARY INFORMATION (SI)

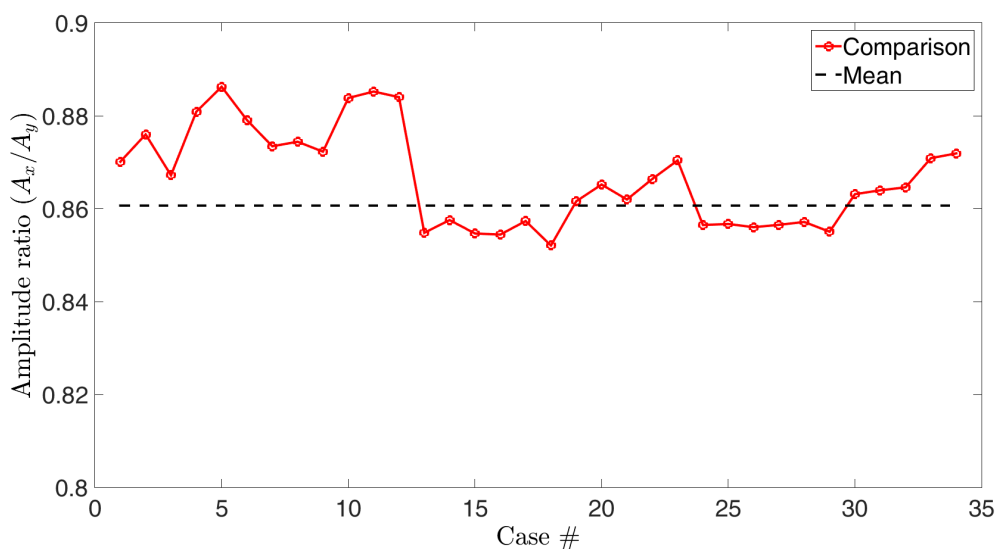


Fig. S1: Plots depicting the amplitude ratio A_x/A_y (Mean value determined for all SSAW (i.e. 2 terminal) cases considered; i.e. Case 14 to 34) for a range of travelling wave and standing wave scenarios determined via curve fitting when compared to a fully coupled LN-fluid system along with the mean value as used in the numerical results. Reference to parameters and dimensions used for each case is listed in Table S1.

^{*}Corresponding author: Laboratory for Micro Systems, Department of Mechanical and Aerospace Engineering, Monash University, Clayton, Victoria 3800, Australia.; E-mail: adrian.neild@monash.edu

The importance of travelling wave components in standing surface acoustic wave (SSAW) systems

Table S1: Case parameters as per produced in Figure S1. Number of interdigital transducer (IDT) terminals denote a travelling wave (TSAW) (i.e. 1) or a standing wave (SSAW) (i.e. 2) scenario. A $h/\lambda_{SAW} = 1/4.8$ was used to compare the streaming fields with that reported by Nama et al.¹ (i.e. $W = \lambda_{SAW}$, $h = 1/4.8$; $\lambda_{SAW} = 600 \mu\text{m}$). All cases are based on a $\lambda_{SAW} = 40 \mu\text{m}$.

Case Number (#)	BC _{imp}	Number of IDT terminals	W/λ_{SAW}	h/λ_{SAW}
1	PDMS	1 (TSAW)	10	1/4.8
2	PDMS	1 (TSAW)	10	1
3	PDMS	1 (TSAW)	10	2.5
4	PDMS	1 (TSAW)	5	1/4.8
5	PDMS	1 (TSAW)	5	1
6	PDMS	1 (TSAW)	5	2.5
7	Water	1 (TSAW)	10	1/4.8
8	Water	1 (TSAW)	10	1
9	Water	1 (TSAW)	10	2.5
10	Water	1 (TSAW)	5	1/4.8
11	Water	1 (TSAW)	5	1
12	Water	1 (TSAW)	5	2.5
13	PDMS	2 (SSAW)	10	1/4.8
14	PDMS	2 (SSAW)	10	1
15	PDMS	2 (SSAW)	10	2.5
16	PDMS	2 (SSAW)	5	1/4.8
17	PDMS	2 (SSAW)	5	1
18	PDMS	2 (SSAW)	5	2.5
19	PDMS	2 (SSAW)	2	1/4.8
20	PDMS	2 (SSAW)	2	1
21	PDMS	2 (SSAW)	2	2.5
22	PDMS	2 (SSAW)	1	1/4.8
23	PDMS	2 (SSAW)	1	1
24	Water	2 (SSAW)	10	1/4.8
25	Water	2 (SSAW)	10	1
26	Water	2 (SSAW)	10	2.5
27	Water	2 (SSAW)	5	1/4.8
28	Water	2 (SSAW)	5	1
29	Water	2 (SSAW)	5	2.5
30	Water	2 (SSAW)	2	1/4.8
31	Water	2 (SSAW)	2	1
32	Water	2 (SSAW)	2	2.5
33	Water	2 (SSAW)	1	1/4.8
34	Water	2 (SSAW)	1	1

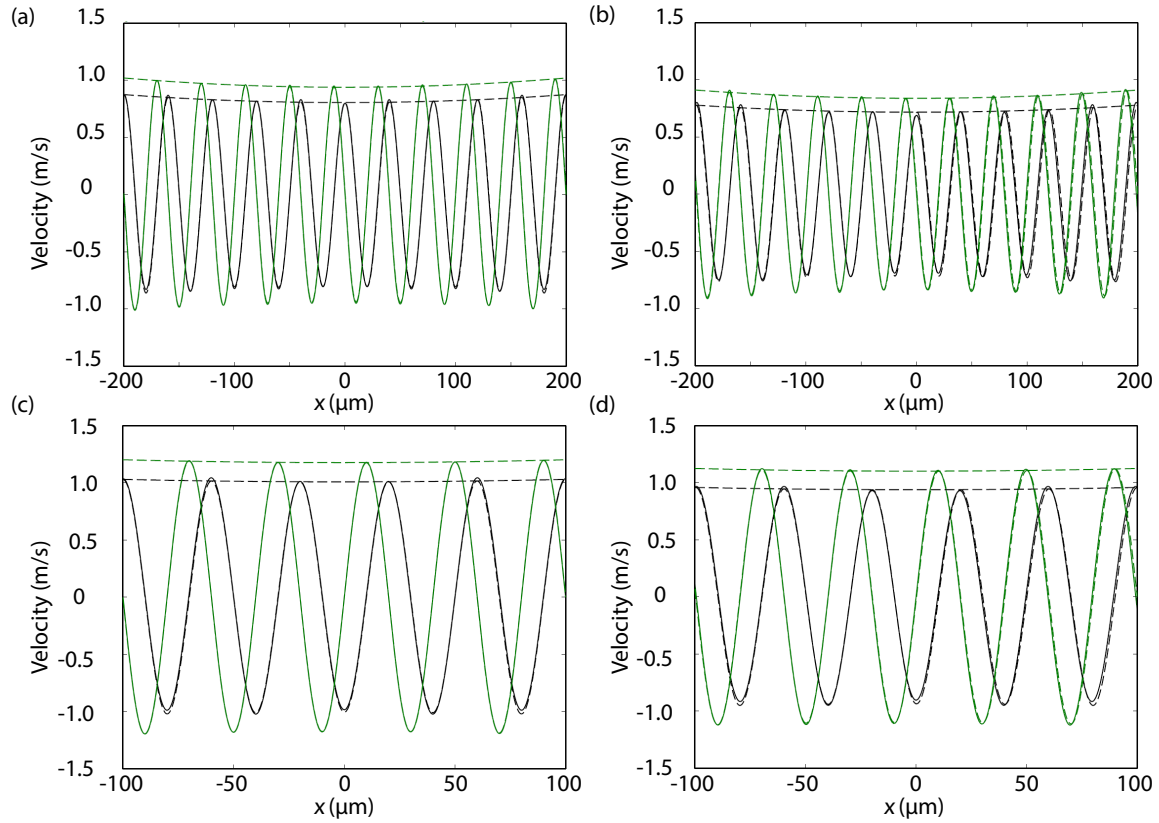


Fig. S2: Plots depicting four specific cases showing the comparison between a fully coupled LN-fluid system against the use of the boundary condition in Equation 16 of the velocity at the LN-fluid interface. Comparisons for a SSAW case with $W = 200 \mu\text{m}$ (i.e. $10 \lambda_{\text{SSAW}}$) (a) $h = 40 \mu\text{m}$ (i.e. $1 \lambda_{\text{SSAW}}$; Case Number 14) (b) $h = 100 \mu\text{m}$ (i.e. $2.5 \lambda_{\text{SSAW}}$; Case Number 15) and with a $W = 100 \mu\text{m}$ (i.e. $5 \lambda_{\text{SSAW}}$) (c) $h = 40 \mu\text{m}$ (i.e. $1 \lambda_{\text{SSAW}}$; Case Number 17) (d) $h = 100 \mu\text{m}$ (i.e. $2.5 \lambda_{\text{SSAW}}$; Case Number 18). The y component velocity u_y , is denoted by the green line and the x component velocity u_x , is denoted by the black line. Solid lines represent the fully coupled model results and the dashed lines represent the fitted data along with the decay C_d , denoted on top of each curve.
 Note: Reference to parameters and dimensions used for each case is listed in Table S1.

REFERENCES

- [1] N. Nama, R. Barnkob, Z. Mao, C. J. Kähler, F. Costanzo and T. J. Huang, *Lab on a Chip*, 2015, **15**, 2700–2709.

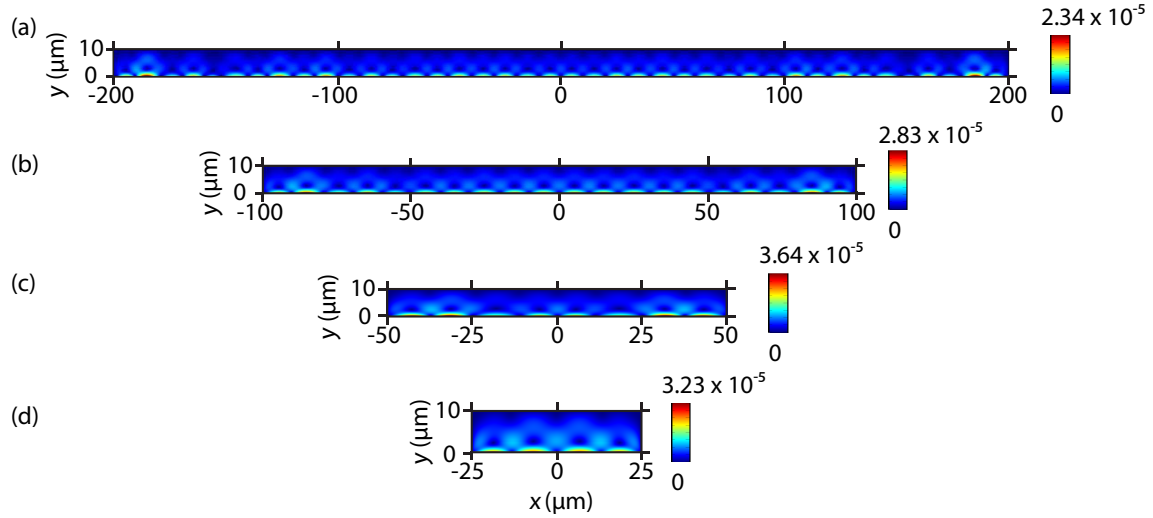


Fig. S3: Resultant plots for a $\lambda_{SAW} = 40 \mu\text{m}$ and $10 \mu\text{m}$ high (i.e. $h = 10 \mu\text{m}$; $0.25 \lambda_{SAW}$) with a PDMS impedance boundary condition on the side walls and upper boundary. Surface plots represent the streaming velocity field $\langle v_2 \rangle$ for varying channel widths, (a) $W = 400 \mu\text{m}$ (i.e. $W = 10 \lambda_{SAW}$), (b) $W = 200 \mu\text{m}$ (i.e. $W = 5 \lambda_{SAW}$), (c) $W = 80 \mu\text{m}$ (i.e. $W = 2 \lambda_{SAW}$) and (d) $W = 40 \mu\text{m}$ (i.e. $W = \lambda_{SAW}$)

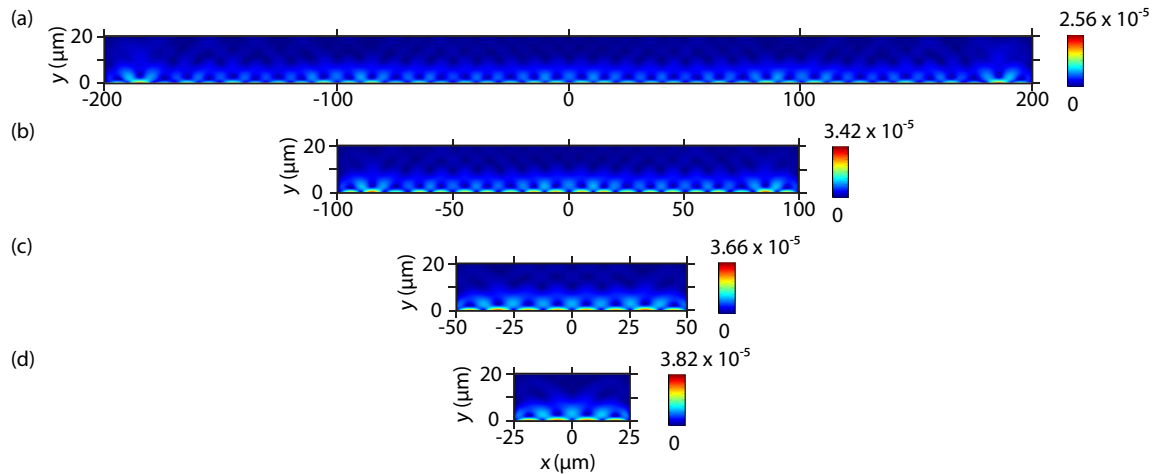


Fig. S4: Resultant plots for a $\lambda_{SAW} = 40 \mu\text{m}$ and $20 \mu\text{m}$ high (i.e. $h = 20 \mu\text{m}$; $0.5 \lambda_{SAW}$) with a PDMS impedance boundary condition on the side walls and upper boundary. Surface plots represent the streaming velocity field $\langle v_2 \rangle$ for varying channel widths, (a) $W = 400 \mu\text{m}$ (i.e. $W = 10 \lambda_{SAW}$), (b) $W = 200 \mu\text{m}$ (i.e. $W = 5 \lambda_{SAW}$), (c) $W = 80 \mu\text{m}$ (i.e. $W = 2 \lambda_{SAW}$) and (d) $W = 40 \mu\text{m}$ (i.e. $W = \lambda_{SAW}$)

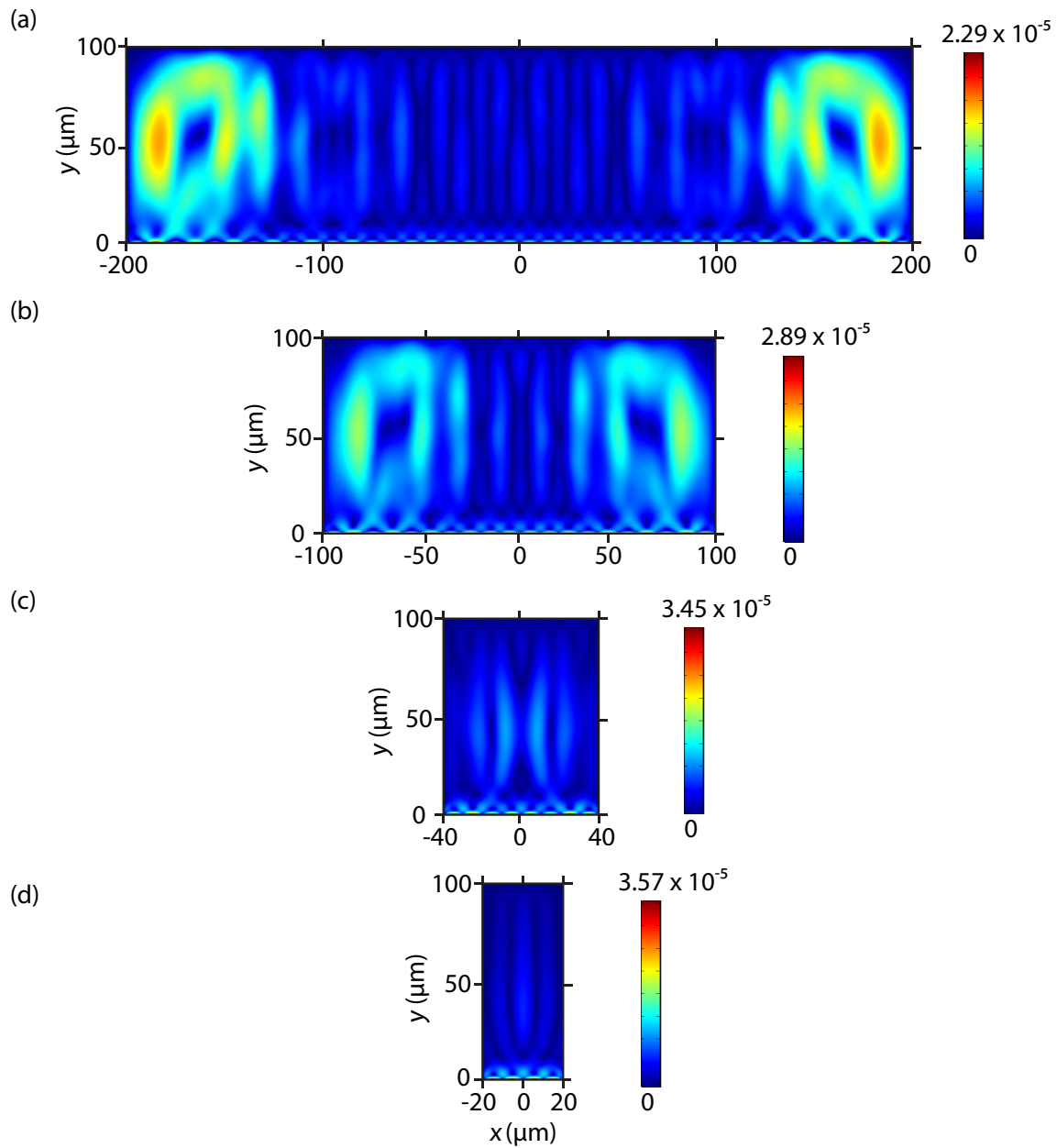


Fig. S5: Resultant plots for a $\lambda_{SAW} = 40 \mu\text{m}$ and $100 \mu\text{m}$ high (i.e. $h = 100 \mu\text{m}$; $2.5 \lambda_{SAW}$) with a PDMS impedance boundary condition on the side walls and upper boundary. Surface plots represent the streaming velocity field $\langle v_2 \rangle$ for varying channel widths, (a) $W = 400 \mu\text{m}$ (i.e. $W = 10 \lambda_{SAW}$), (b) $W = 200 \mu\text{m}$ (i.e. $W = 5 \lambda_{SAW}$), (c) $W = 80 \mu\text{m}$ (i.e. $W = 2 \lambda_{SAW}$) and (d) $W = 40 \mu\text{m}$ (i.e. $W = \lambda_{SAW}$)

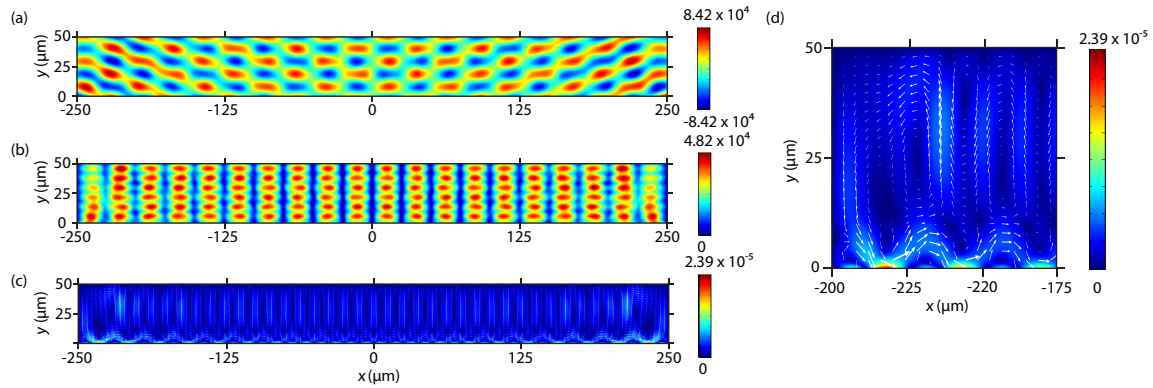


Fig. S6: Resultant plots for a $\lambda_{SAW} = 50 \mu\text{m}$, $50 \mu\text{m}$ high and $500 \mu\text{m}$ wide chamber (i.e. $W = 500 \mu\text{m}$ and $h = 50 \mu\text{m}$) with a PDMS impedance boundary condition on the side walls and upper boundary. Surface plots represent the (a) first-order pressure fields, P_1 (b) time-averaged second-order pressure fields, $\langle P_2 \rangle$ and (c) streaming velocity field $\langle v_2 \rangle$ and (d) a zoomed in surface plots of the resultant streaming velocity field, $\langle v_2 \rangle$ at the left hand side of the channel to illustrate the observed streaming rolls. Velocity field vectors are depicted with white arrows.

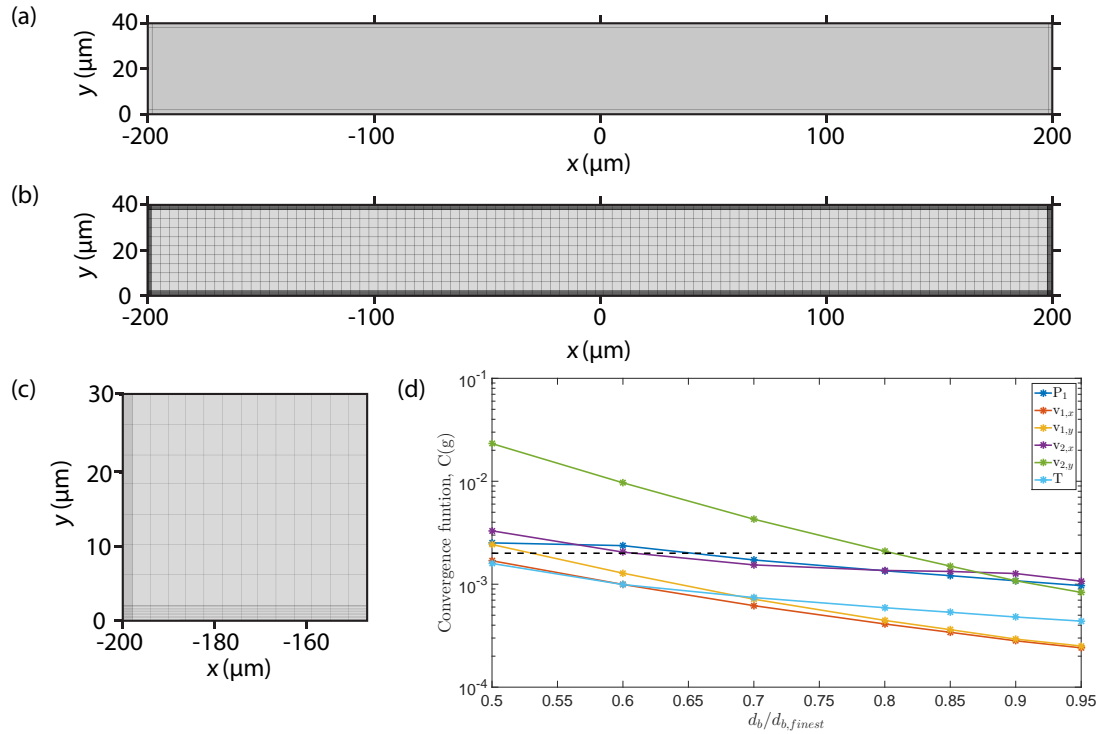


Fig. S7: Mesh distribution for a $400 \mu\text{m}$ wide and $40 \mu\text{m}$ high channel (i.e. $W = 400 \mu\text{m}$; $h = 40 \mu\text{m}$), (a) depicting the sectioning done consisting of a $2 \mu\text{m}$ wide section at each side of the rectangular chamber, (b) an example mesh distribution consisting of boundary mesh elements, $d_b = 4 \mu\text{m} \times 0.2 \mu\text{m}$ and (c) a zoomed in view of the bottom left corner of the rectangular geometry. (d) Mesh convergence analysis carried out to satisfy a convergence, $C(g) = 0.002$ (Depicted with a black dashed line).

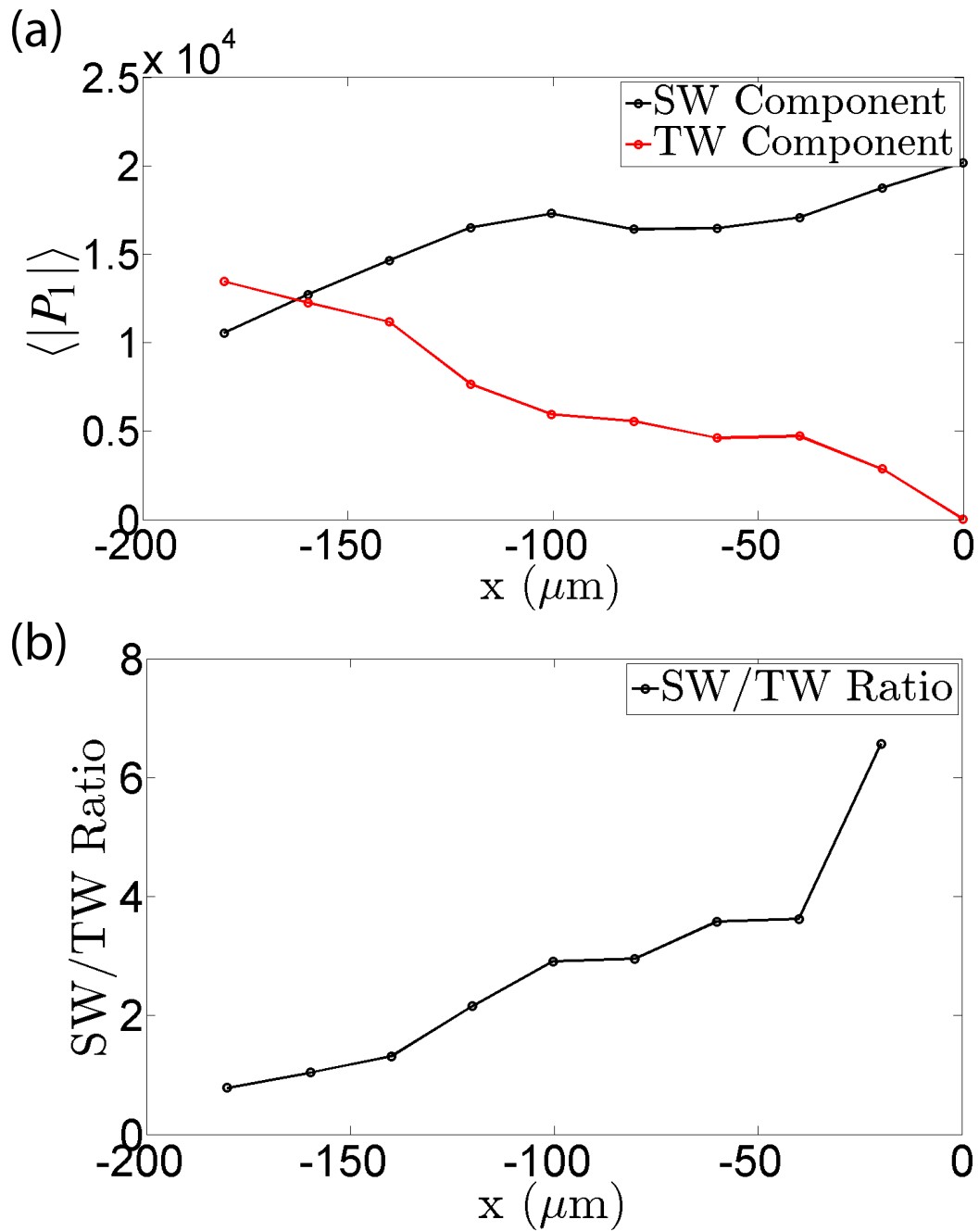


Fig. S8: Line plots describing the TW to SW ratio at $y = 5 \mu\text{m}$, where (a) the time-averaged absolute pressure, $\langle |P_1| \rangle$ against position x of the TW and SW components individually in μm (b) The SW to TW ratio at the local pressure minima locations in the x -direction.

Note: All demonstrated values correspond the left half of the channel width (i.e. $x = -200 \mu\text{m} : 0 \mu\text{m}$) and are symmetrical about $x = 0 \mu\text{m}$. The SW/TW ratio is not shown for the node in the centre of the channel (i.e. $x = 0 \mu\text{m}$) as it would skew the other values, registering a SW/TW ratio of 1.4987×10^{12} .